Optics Letters

Low-threshold lasing at 1975 nm in thulium-doped tellurite glass microspheres

Francis Vanier,[1,*] François Côté,[2] Mohammed El Amraoui,[2] Younès Messaddeq,[2] Yves-Alain Peter,[1] and Martin Rochette[3]

[1]Department of Engineering Physics, Polytechnique Montréal, Montréal, Québec H3C 3A7, Canada
[2]Center for Optics, Photonics and Lasers (COPL), Laval University, Québec City, Québec G1V 0A6, Canada
[3]Department of Electrical and Computer Engineering, McGill University, Montréal, Québec H3A 2A7, Canada
*Corresponding author: francis-2.vanier@polymtl.ca

Received 12 August 2015; revised 2 October 2015; accepted 10 October 2015; posted 12 October 2015 (Doc. ID 247825); published 5 November 2015

Thulium-doped (Tm-doped) tellurite glass microspheres are used as laser media. Emission lines at wavelengths near 1975 nm are observed. The onset of laser emission is achieved with 8.6 and 30 μW of coupled pump power and injected pump power, respectively, at a wavelength of 1554 nm. To the authors' knowledge, these are the lowest laser threshold values recorded for a Tm-doped tellurite glass microcavity. Intrinsic *Q*-factors above 10^6 for the undoped tellurite glass microspheres assert the quality of the fabrication processes. An optical intrinsic *Q*-factor comparison between Tm-doped tellurite and undoped tellurite microspheres shows that ion absorption is the dominant loss source at pump wavelengths. Lower lasing threshold powers and higher power conversion are observed at longer pump wavelengths in agreement with theoretical models. © 2015 Optical Society of America

OCIS codes: (140.3945) Microcavities; (140.3410) Laser resonators; (140.3070) Infrared and far-infrared lasers; (060.2290) Fiber materials.

http://dx.doi.org/10.1364/OL.40.005227

Thulium-based lasers emitting near a wavelength of 2 μm are used in many applications, such as laser-assisted medical interventions [1–3], material analysis [4], gas detection [5], and optical telecommunications [6].

To support these applications, the use of tellurite glasses as a host material is attractive, owing to its transparency in the 1.8–2.1 μm region. Tellurite glasses also enable dissolving a larger concentration of thulium ions compared to other mid-IR glasses, such as chalcogenides. As a tellurite glass, Tm-doped TeO_2-ZnO-Na_2O-$ZnCl_2$ glass has previously shown larger absorption and emission cross sections in the $^3F_4 \rightarrow {}^3H_6$ transition region compared to silica glass [7–9]. Most of the Tm-doped tellurite glass laser media are fiber-based and provide relatively high power output but exhibit high power threshold [9].

Whispering gallery mode (WGM) cavities, such as microspheres, are ideal laser media, as they are compact, they can achieve high *Q*-factors, and they have small optical-mode volumes. Lasing in doped WGM cavities was previously shown, for example, in Er-doped silica, tellurite glass [10–12], and Er–Yb codoped tellurite glass [13], among others. While WGM lasers' output power is usually below 1 mW, they exhibit threshold power of a few microwatts and efficient power conversion.

Threshold pump powers of 0.5 mW and up were shown in Tm-doped tellurite microspheres [14–16]. It is expected that the cavity *Q*-factor could be increased by using spheres of improved glass transmittance, leading to a laser threshold of a few microwatts typically observed in doped WGM microcavities [10,11]. In Tm-doped silica microspheres, for example, an estimated threshold pump power of 50 μW was reported for near 2 μm emission [17].

In this Letter, we report lasing emission at 1975 nm of Tm-doped tellurite glass microspheres. The threshold pump power of 30 μW for a pump wavelength of 1554 nm is the lowest ever reported for a Tm-doped tellurite microcavity by at least an order of magnitude [14–16]. Microwatt laser threshold values were achieved from microspheres with intrinsic *Q*-factors above 10^6, owing to the high purity and transparency of the host glass.

The microspheres are made from a Tm-doped tellurite glass fiber. The glass is produced from high-purity oxide and carbonate (Na_2CO_3) powders (>99.99%) dried separately at a high temperature and mixed together as 74TeO_2-15ZnO-5Na_2O-5$ZnCl_2$-1Tm_2O_3 (mol. %). A second drying step is performed where the $ZnCl_2$ compound acts as a drying agent. The glass synthesis is done at 800°C during 1 h. The melted glass is then transferred to a fiber preform and slowly cooled down to 290°C to prevent crystallization. Finally, the preform is pulled into a monoindex optical fiber with a diameter of 210 μm. An undoped fiber and microspheres were also fabricated using similar techniques for comparison. The dopant concentration N_T is $(4.2 \pm 0.3) \times 10^{20}$ ions/cm^3.

The microspheres are fabricated using a two-step process. The tellurite fiber is first tapered to a 10 μm tip using a high-power CO_2 laser. With additional laser pulses, the tip transforms into a microsphere due to surface tension. A silica-tapered fiber

is used to couple light in and out of the microsphere. The microsphere and the tapered fiber are encapsulated in a glass tube to prevent contamination and the reduction of the Q-factor as discussed in [18].

Figure 1(a) presents the setup used to measure the Q-factors and the laser emission of the microspheres. The emission of a tunable laser source (TLS, Keysight 81600B) is sent to the microsphere using a silica-tapered fiber with a diameter of 2 μm. An optical spectrum analyzer (OSA, Yokogawa AQ6375) measures the transmitted pump signal and the forward laser emission. A part of the injected pump signal is measured with an optical detector (DET). Finally, a polarization controller (PC) is used to optimize the coupling conditions. Figure 1(b) shows the image of a typical tellurite glass microsphere.

To measure the transmission spectra and the loaded Q-factors, the wavelength of the tunable laser is scanned over 1 nm near the wavelengths of 1504, 1554, 1585, and 1629 nm. The OSA is set to zero-span mode with a bandwidth of 2 nm. The narrower resonances were identified for each spectral region, and a Lorentzian fit was used to determine the loaded Q-factors. A low power pump signal of 800 nW was used to prevent any thermal drifting. For the doped microspheres, additional care was taken to ensure that the Q-factor measurements were not affected by ion absorption intensity dependence, i.e., with an injected power 25 times lower than the threshold power. The diameters of the doped and undoped spheres are approximately 30 μm.

Figure 2 presents the intrinsic Q-factors, Q_0, of undoped (black diamonds) and doped (red circles) microspheres for an undercoupled regime. The undoped microspheres' resonances exhibit similar Q_0 of $\sim 2 \times 10^6$ between 1500 and 1630 nm, as expected. On the contrary, the doped spheres' resonances suffer increasing losses at longer wavelengths. The comparison between the doped tellurite and the undoped tellurite Q-factors shows that the losses can be attributed to the dopant absorption. Following the WGM laser model of [11,19], the intrinsic Q-factor, Q_0^{Tm}, related to the low pump power losses caused by ion absorption can be calculated as

$$Q_0^{\mathrm{Tm}} = \frac{m_p}{R_c \sigma_{a,p}} \frac{\int_S |\vec{e_p}|^2 \mathrm{d}S}{\int_S N_T |\vec{e_p}|^2 \mathrm{d}S} \approx \frac{m_p}{R_c \sigma_{a,p} N_T}, \quad (1)$$

where m_p is the azimuthal number of the pump mode, $\sigma_{a,p}$ is the ion absorption cross section at the pump wavelength, R_c is the sphere radius, and N_T is the ion concentration. The approximation is valid, because the evanescent field outside the cavity is negligible compared to the optical field inside. Using Eq. (1), the absorption cross-section values of [8,9], and the undoped tellurite Q_0 values, theoretical Q_0 can be found for $R_c = 15$ μm and $N_T = 4.2 \times 10^{20}$ ions/cm^3. They are

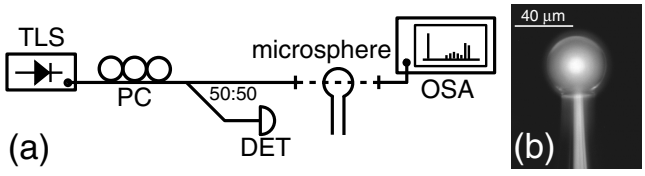

Fig. 1. (a) Experimental setup for Tm-doped tellurite glass microsphere laser emission. TLS, tunable laser source; PC, polarization controller; DET, optical detector; OSA, optical spectrum analyzer. (b) Microscope image of a typical tellurite microsphere.

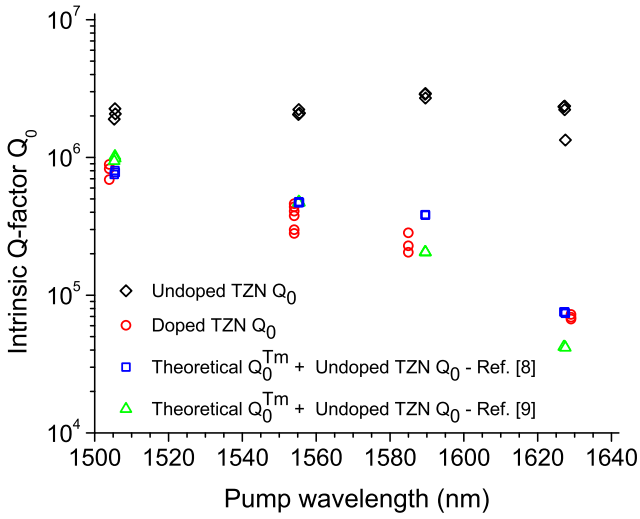

Fig. 2. Intrinsic Q-factor Q_0 for undoped tellurite spheres (black diamonds) and Tm-doped tellurite spheres (red circles) for an undercoupled regime. Theoretical intrinsic Q_0^{Tm} following absorption cross-section values of [8,9] is also shown.

plotted in Fig. 2 (blue rectangles and green triangles). The decreasing Q-factor with longer wavelengths arises mainly from the increasing absorption cross section of thulium [8,9] as presented in Fig. 6. Figure 3 shows the forward emission spectrum of a Tm-doped microsphere using the *Hold Max* feature of the OSA as the pump wavelength is continuously scanned from 1554 to 1555 nm with a pump power of 86 μW. The *Hold Max* feature cumulates the emission spectra resulting from the successive excitation of resonances scanned by the pump laser. The photoluminescence of the Tm ions is filtered by the cavity resonances. It is visible from 1775 to 2000 nm and is centered around a wavelength of 1900 nm. It displays a free spectral range of successive azimuthal order modes of 20.4 nm, which is associated with a cavity radius of ~14 μm, in agreement with visual inspection of the sphere. Laser emission lines are also measured and are centered at wavelengths around

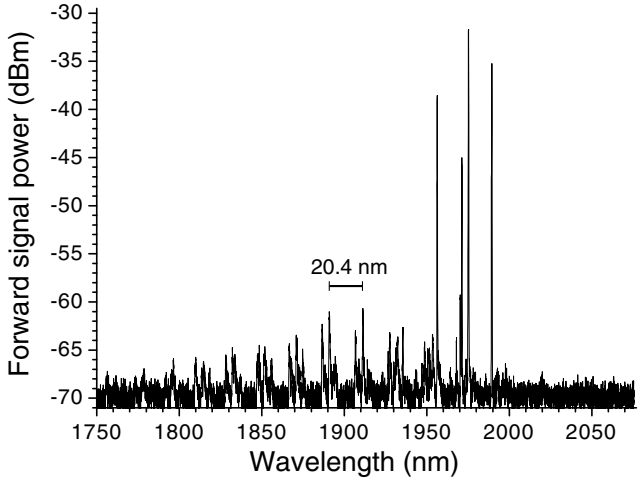

Fig. 3. Forward emission spectrum of a Tm-doped tellurite glass microsphere. The photoluminescence of the Tm ions is filtered by the cavity resonances. Multimode laser emission lines are also visible and are centered at a wavelength of 1975 nm.

1975 nm. The emission is multimode, because many modes achieve lasing threshold conditions. These modes usually have high Q-factors and a good field overlap with the pump mode. Laser lines occur at the long-wavelength side of the photoluminescence spectrum due to the large thulium ion concentration. The laser signal gets absorbed and reemits to longer wavelengths following a nonradiative decay in the $^3F_4$ band [15,20].

Three threshold curves are presented in Fig. 4 for three different pump resonances near a wavelength of 1554 nm. The measurement technique is similar to [21,22]. Similarly to the Q-factor measurements, the OSA is used in zero-span mode, and its measurement bandwidth of 2 nm is centered on the strongest emission peak at a wavelength of 1975 nm. A linear fit is used to extract the lasing threshold coupled power and the efficiency of the emission process. Each curve has a different threshold value $P_{p,\mathrm{th}}^{\mathrm{coup}}$ of 8.6, 17.2, and 25 μW and internal efficiency $\eta_{\mathrm{in}} = dP_s/dP_p^{\mathrm{coup}}$ of 4%, 3%, and 1.6%, respectively. This is due to their different intrinsic Q-factors, coupling conditions, and mode overlaps with the signal mode at 1975 nm. Based on their resonance's transmission T, all the curves have similar threshold-injected powers $P_p^{\mathrm{in}} = P_p^{\mathrm{coup}}/(1-T)$ of ∼30 μW. These coupled and injected power values are the lowest measured for a Tm-doped tellurite glass microcavity to the authors' knowledge.

Since the ion absorption cross section depends strongly on the pump wavelength, it is interesting to see how it affects the threshold power and the lasing efficiency. Figure 5 presents the forward signal power as a function of the coupled pump power for three different pump modes, each near different pump wavelengths of 1504, 1554, 1585, and 1629 nm. The threshold coupled pump power $P_{p,\mathrm{th}}^{\mathrm{coup}}$ and the internal efficiency η_{in} tend to be lower and higher, respectively, at a longer wavelength where the ion absorption cross section is more important.

Both can be calculated as [11,19]

$$\eta_{\mathrm{in}} = \frac{m_p^2\omega_s^3}{m_s^2\omega_p^3}\frac{N_s|\vec{e_p}|^2_{\max}}{N_p|\vec{e_s}|^2_{\max}}\frac{\tau_s}{\tau_{s,c}}\frac{\gamma_p^{\mathrm{Tm}}}{\left(\gamma_p^{\mathrm{Tm}}+\frac{1}{2\tau_{p,0}}\right)}, \tag{2}$$

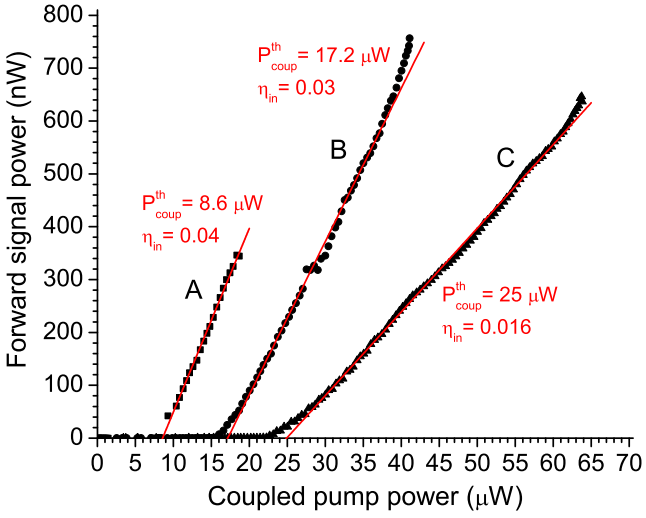

Fig. 4. Forward signal power at a wavelength of 1975 nm versus the coupled pump power. The input pump power is 86 μW. Curves A, B, and C represent different pump resonances near a wavelength of 1554 nm.

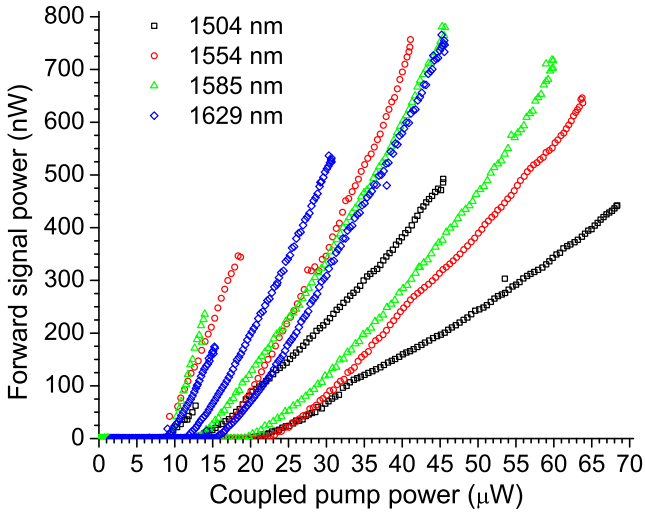

Fig. 5. Forward signal power at a wavelength of 1975 nm versus the coupled pump power near wavelengths of 1504 nm (black squares), 1554 nm (red circles), 1585 nm (green triangles), and 1629 nm (blue diamond). For each pump wavelength region, three curves represent different pump resonances.

$$P_{p,\mathrm{th}}^{\mathrm{coup}} = \frac{2\hbar R_c}{c^2\tau_{\mathrm{Tm}}[\sigma_{a,s}+\sigma_{e,s}]} \times\left(\frac{N_T\omega_s\tau_s R_c\sigma_{a,s}}{m_s}+1\right)\frac{\omega_s^2}{m_s\tau_{s,c}}\frac{N_s}{|\vec{e_s}|^2_{\max}}\frac{1}{\eta_{\mathrm{in}}}, \tag{3}$$

where $N_{p,s} = \int_V n_0^2(\vec{r})|\vec{e}_{p,s}|^2 dV$ are the normalization factors and $|\vec{e}_{p,s}|^2_{\max}$ are the maximum values of $|\vec{e}_{p,s}|^2$ for the pump and emitted signal, respectively; $n_0(\vec{r})$ is the refractive index profile; and $\omega_{p,s}$ are the pump/signal frequencies. $\tau_{s,c}$, $\tau_{p,0}$, and $\tau_{\mathrm{Tm}} \approx 1.35$ ms are the decay time of the signal coupling losses, the decay time of the pump intrinsic losses, and the ion lifetime of the $^3F_4 \rightarrow {}^3H_6$ transition related to the ion concentration [8]. $\tau_s = (1/\tau_{s,0} + 1/\tau_{s,c})^{-1}$ is the total decay time of the signal resonance without the gain of the ions. $\sigma_{a(e),p(s)}$ are the ion absorption (emission) cross sections of the pump (signal). $\hbar$ and c are the Planck constant and the speed of light in vacuum. Finally, γ_p^{Tm} is the clamped pump loss rate due to the ion absorption above the lasing threshold, and it is defined by

$$\gamma_p^{\mathrm{Tm}} = -\frac{1}{2\tau_s}\frac{m_s\omega_p}{m_p\omega_s} \times\left(\frac{N_T\omega_s\tau_s R_c[\sigma_{a,s}\sigma_{e,p}-\sigma_{a,p}\sigma_{e,s}]}{m_s[\sigma_{a,s}+\sigma_{e,s}]}+\frac{[\sigma_{a,p}+\sigma_{e,p}]}{[\sigma_{a,s}+\sigma_{e,s}]}\right).$$

As seen in Fig. 2, the pump mode losses are dominated by the ion absorption, while the intrinsic resonator losses such as scattering are constant. This means that γ_p^{Tm} increases, while $\tau_{p,0}$ remains constant at longer wavelengths. Following Eqs. (2) and (3), for similar lasing signal mode characteristics, η_{in} should increase and $P_{p,\mathrm{th}}^{\mathrm{coup}}$ should decrease at longer wavelengths where the thulium absorption cross section is larger. This is in agreement with the experimental results of Fig. 5.

Figure 5 shows the emission power for a signal mode located at 1975 nm, pumped by different pump modes. The signal mode characteristic values such as the coupling Q-factors Q_c and the intrinsic Q-factor Q_0 that excludes the ion gain can

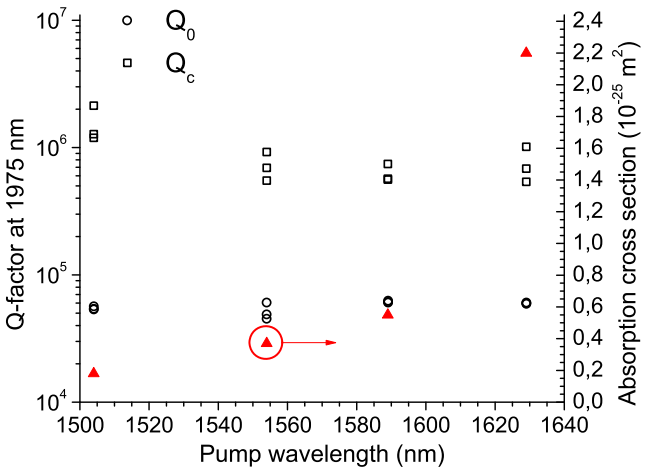

Fig. 6. Signal resonance Q_0 (black circles) and Q_c (black squares) at 1975 nm obtained by fitting their threshold curves at different pump wavelengths for first-order radial modes. The fitted absorption cross sections (red triangles) are also shown.

be extracted from these curves using Eqs. (2) and (3). Figure 6 shows the extracted Q_0 and Q_c for each pump wavelength. As expected, the intrinsic and the coupling Q-factors share similar values near $\sim 6 \times 10^4$ and $\sim 8 \times 10^5$, respectively. The larger variation of the Q_c values can be linked to the undercoupled regime conditions where small variations of the Q_0 values cause large variations of the associated Q_c values. The best results were obtained by using the pump absorption cross section, also shown in Fig. 6. These values are in good agreement with the values from [8,9].

In conclusion, we presented measurements of low-threshold laser emissions at a wavelength of 1975 nm of Tm-doped tellurite glass microspheres. The threshold pump power of 30 μW is the lowest value reported for a Tm-doped microcavity and at least a tenfold improvement for a Tm-doped tellurite microcavity. Different pump wavelengths were used, and the results show better lasing performance at longer pump wavelengths where the ion absorption cross section is larger, in agreement with the theoretical models.

Funding. Canada Excellence Research Chairs, Government of Canada (CERC); Canada Foundation for Innovation (CFI); Fonds de Recherche du Québec-Nature et Technologies (FRQNT) (Equipe 173906); Natural Sciences and Engineering Research Council of Canada (NSERC).

REFERENCES

1. N. S. Nishioka and Y. Domankevitz, IEEE J. Quantum Electron. **26**, 2271 (1990).
2. N. J. Scott, C. M. Cilip, and N. M. Fried, IEEE J. Sel. Top. Quantum Electron. **15**, 435 (2009).
3. R. L. Blackmon, P. B. Irby, and N. M. Fried, J. Biomed. Opt. **16**, 071403 (2011).
4. M. Baudelet, C. C. C. Willis, L. Shah, and M. Richardson, Opt. Express **18**, 7905 (2010).
5. K. Bremer, A. Pal, S. Yao, E. Lewis, R. Sen, T. Sun, and K. T. V. Grattan, Appl. Opt. **52**, 3957 (2013).
6. Z. Li, A. M. Heidt, J. M. O. Daniel, Y. Jung, S. U. Alam, and D. J. Richardson, Opt. Express **21**, 9289 (2013).
7. E. R. Taylor, L. N. Ng, N. P. Sessions, and H. Buerger, J. Appl. Phys. **92**, 112 (2002).
8. H. Gebavi, D. Milanese, R. Balda, S. Chaussedent, M. Ferrari, J. Fernandez, and M. Ferraris, J. Phys. D **43**, 135104 (2010).
9. B. Richards, A. Jha, Y. Tsang, D. Binks, J. Lousteau, F. Fusari, A. Lagatsky, C. Brown, and W. Sibbett, Laser Phys. Lett. **7**, 177 (2010).
10. V. Sandoghdar, F. Treussart, J. Hare, V. Lefèvre-Seguin, J.-M. Raimond, and S. Haroche, Phys. Rev. A **54**, R1777 (1996).
11. B. Min, T. J. Kippenberg, L. Yang, K. J. Vahala, J. Kalkman, and A. Polman, Phys. Rev. A **70**, 033803 (2004).
12. X. Peng, F. Song, M. Kuwata-Gonokami, S. Jiang, and N. Peyghambarian, Opt. Eng. **44**, 124402 (2005).
13. Y. Ruan, K. Boyd, H. Ji, A. Francois, H. Ebendorff-Heidepriem, J. Munch, and T. M. Monro, Opt. Express **22**, 11995 (2014).
14. K. Sasagawa, Z. Yonezawa, R. Iwai, J. Ohta, and M. Nunoshita, Appl. Phys. Lett. **85**, 4325 (2004).
15. J. Wu, S. Jiang, T. Qua, M. Kuwata-Gonokami, and N. Peyghambarian, Appl. Phys. Lett. **87**, 211118 (2005).
16. J. Wu, S. Jiang, and N. Peyghambarian, Opt. Express **13**, 10129 (2005).
17. A. Pal, S. Y. Chen, R. Sen, T. Sun, and K. T. V. Grattan, Laser Phys. Lett. **10**, 085101 (2013).
18. F. Vanier, Y.-A. Peter, and M. Rochette, Opt. Express **22**, 28731 (2014).
19. C. R. Giles and E. Desurvire, J. Lightwave Technol. **9**, 271 (1991).
20. J. Li, Z. Sun, H. Luo, Z. Yan, K. Zhou, Y. Liu, and L. Zhang, Opt. Express **22**, 5387 (2014).
21. G. Lin, Y. Candela, O. Tillement, Z. Cai, V. Lefèvre-Seguin, and J. Hare, Opt. Lett. **37**, 5193 (2012).
22. F. Vanier, M. Rochette, N. Godbout, and Y.-A. Peter, Opt. Lett. **38**, 4966 (2013).